

Measuring nucleus mechanics within a living multicellular organism: Physical decoupling and attenuated recovery rate are physiological protective mechanisms of the cell nucleus under high mechanical load

Noam Zuela-Sopilniak^a, Daniel Bar-Sela^b, Chayki Charar^a, Oren Wintner^b, Yosef Gruenbaum^{a,*}, and Amnon Buxboim^{b,c,*}

^aDepartments of Genetics and ^bCell and Developmental Biology, The Alexander Silberman Institute of Life Sciences, Hebrew University of Jerusalem, Jerusalem 9190401, Israel; ^cAlexander Grass Center for Bioengineering, The Rachel and Selim Benin School of Computer Science and Engineering, The Hebrew University of Jerusalem, Jerusalem 9190416, Israel

ABSTRACT Nuclei within cells are constantly subjected to compressive, tensile, and shear forces, which regulate nucleoskeletal and cytoskeletal remodeling, activate signaling pathways, and direct cell-fate decisions. Multiple rheological methods have been adapted for characterizing the response to applied forces of isolated nuclei and nuclei within intact cells. However, *in vitro* measurements fail to capture the viscoelastic modulation of nuclear stress-strain relationships by the physiological tethering to the surrounding cytoskeleton, extracellular matrix and cells, and tissue-level architectures. Using an equiaxial stretching apparatus, we applied a step stress and measured nucleus deformation dynamics within living *Caenorhabditis elegans* nematodes. Nuclei deformed nonmonotonically under constant load. Nonmonotonic deformation was conserved across tissues and robust to nucleoskeletal and cytoskeletal perturbations, but it required intact linker of nucleoskeleton and cytoskeleton complex attachments. The transition from creep to strain recovery fits a tensile-compressive linear viscoelastic model that is indicative of nucleoskeletal–cytoskeletal decoupling under high load. Ce-lamin (*lmn-1*) knockdown softened the nucleus, whereas nematode aging stiffened the nucleus and decreased deformation recovery rate. Recovery lasted minutes rather than seconds due to physiological damping of the released mechanical energy, thus protecting nuclear integrity and preventing chromatin damage.

Monitoring Editor

Dennis Discher
University of Pennsylvania

Received: Jan 31, 2020

Revised: May 26, 2020

Accepted: Jun 8, 2020

This article was published online ahead of print in MBoC in Press (<http://www.molbiolcell.org/cgi/doi/10.1091/mbc.E20-01-0085>) on June 17, 2020.

*Address correspondence to: Yosef Gruenbaum (gru@vms.huji.ac.il); Amnon Buxboim (amnon.buxboim@mail.huji.ac.il).

Abbreviations used: HGPS, Hutchinson-Gilford progeria syndrome; KLH, keyhole limpet hemocyanin; LINC, linker of nucleoskeleton and cytoskeleton; NCD, nucleoskeletal–cytoskeletal decoupling; NGM, nematode growth medium; ROI, region of interest; SLS, standard linear solid model.

© 2020 Zuela-Sopilniak et al. This article is distributed by The American Society for Cell Biology under license from the author(s). Two months after publication it is available to the public under an Attribution–Noncommercial–Share Alike 3.0 Unported Creative Commons License (<http://creativecommons.org/licenses/by-nc-sa/3.0>).

“ASCB®,” “The American Society for Cell Biology®,” and “Molecular Biology of the Cell®” are registered trademarks of The American Society for Cell Biology.

INTRODUCTION

The viscoelastic properties of the nucleus are required to protect the genetic material from applied forces (Furusawa et al., 2015) while permitting flexibility to allow constricted cell migration (Denais et al., 2016; Raab et al., 2016; Irianto et al., 2017) and mechanosensitivity (Athirasala et al., 2017). Externally applied and cell-generated forces propagate along cytoskeletal filaments and are transmitted to the nuclear lamina across linker of nucleoskeleton and cytoskeleton (LINC) complexes. In response to tensile forces that are transmitted to the nuclear lamina across LINC attachments, the nucleus becomes stiffer concomitantly with tyrosine phosphorylation of the nuclear envelope protein emerin (Guilluy et al., 2014). Forces

pulling on the nuclear lamina are transduced into biochemical cues via tension-suppressed phosphorylation-mediated disassembly and turnover of lamin-A filaments (Buxboim *et al.*, 2014), which scale with tissue stiffness (Swift *et al.*, 2013b). Applied forces were also shown to up-regulate transcription rate by stretching chromatin, thus acting directly independent of molecular relays (Tajik *et al.*, 2016).

Multiple complementary rheological methods have been employed for measuring the stress-strain relationship of amphibian and mammalian cell nuclei over a range of deformation length scales and dynamic profiles (Stephens *et al.*, 2018). Indentation experiments of isolated nuclei (Lherbette *et al.*, 2017) and nuclei within adhering cells (Krause *et al.*, 2013) highlighted the stiffness rendered by condensed chromatin, with contributions from linker DNA and internucleosomal interaction (Shimamoto *et al.*, 2017). Micro-manipulation techniques that typically apply intermediate strains separate between small deformation regime dominated by chromatin and large deformations that are resisted by strain stiffening of the lamina (Stephens *et al.*, 2017). Compared with indentation and micro-manipulation techniques, micropipette aspiration induces large deformations (Gonzalez-Bermudez *et al.*, 2019; Hochmuth, 2000). Nuclei responded to applied suction as a viscoelastic solid (Guilak *et al.*, 2000; Rowat *et al.*, 2005) spanning over a broad spectrum of timescales (Dahl *et al.*, 2005) showing decreased deformability with cell differentiation (Pajeroski *et al.*, 2007). Viscous and elastic contributions were affiliated with A- and B-type lamins, respectively (Swift *et al.*, 2013a; Wintner *et al.*, 2020).

In vitro mechanical characterization of isolated nuclei and nuclei within cells has made fundamental contributions. However, these studies cannot account for the modulating effects of the multiscale physiological surroundings that consist of the cytoskeleton, the cell cortex and membrane, the extracellular environment of cells and matrix, and tissue architectures. Already within intact cells, nucleus stiffening was shown to increase cytoskeletal strain by serving as a stress concentrator (Heo *et al.*, 2016). In turn, the physical tethering with the cytoskeleton effectively stiffens the nucleus and slows down the release rate of the stored mechanical energy (Wang *et al.*, 2018).

To measure the strain-stress relationship of the nucleus within its physiological multicellular settings, we performed a creep test of living *Caenorhabditis elegans* nematodes. Nematodes were placed in between two membranes, stretched equiaxially, and nucleus deformation dynamics was recorded. Counter to the whole nematodes and cells within tissue, nuclei exhibited a nonmonotonic response under constant load. Once critical strain was reached, the nucleus transitioned from creep to strain recovery. This anomalous response was conserved across tissues, cytoskeletal perturbations, and nuclear perturbations, yet it required intact LINC attachments. We propose a linear viscoelastic model that superimposes apical compression and tensile stretching. Physical decoupling at high load relaxes tensile stretching, thus giving rise to partial recovery of nuclear deformations over timescales that are set by nuclear viscoelasticity. *Lmn-1* knockdown increased dissipative recovery time and softened nucleus resistance to continuous stresses but had no effect on instantaneous elasticity. Despite maintaining constant Ce-lamin protein level, nuclear resistance to applied load became stiffer and deformation recovery became slower with aging. Nuclei responded within minutes—much slower than in vitro recovery timescales over seconds. Hence, the physiological surroundings of the cytoskeleton, extracellular matrix and cells, and tissue architectures attenuate the release rate of the mechanical energy stored within the nucleus, thus protecting the nuclear envelope and the genetic material from mechanical damage.

RESULTS

Creep test of live nematodes reveals nonmonotonic nuclear response to applied stresses

Measuring nucleus mechanics within live nematodes was performed using a custom-made device constructed based on a former cell stretcher design (Lammerding and Lee, 2009) and mounted onto an inverted epifluorescence microscope (Figure 1A). Live nematodes were placed in between two parallel silicon membranes and immersed in M9 buffer. Pulling the two parallel membranes downward against a static cylinder generated an in-plane uniform and homogeneous equibiaxial tensile strain as calculated by tracking the relative displacements of distinct defects. The deformation dynamics of the nematodes was recorded before and during membrane stretching by time-lapse phase contrast and fluorescence imaging (Figure 1B). Similarly, the deformation dynamics of nuclei within different tissues was evaluated by time-lapse recording of a GFP-fused Ce-lamin fluorescence signal (Figure 1C).

We characterized the mechanical response of worms, cells, and nuclei to applied stresses using creep test rheology. Specifically, we pulled the membranes at ~70% equibiaxial strain and maintained load for 24 min (Figure 1D, i). As a result, the nematodes were stretched longitudinally but not perpendicular to the main axis of the worm due to their thin cylindrical geometry (Figure 1D, ii). The nematodes responded elastically to applied stress: instantaneous deformation at $t = 0$, which was maintained as long as the membranes were held stretched. To evaluate the axial deformation of cells, we estimated the distances between the centers of consecutive pairs of segmented nuclei within the obliquely striated myofibrillar lattice of the body wall muscle tissue (Gettner *et al.*, 1995). Nuclear areal strain dynamics was also evaluated using the segmented GFP-signal regions of interest (ROIs). Both cell and nucleus strains were normalized by worm strains to compensate for differences in the forces that were applied within different nematodes. We found that cells responded elastically to applied stresses just like the nematodes (Figure 1D, iii). However, nuclei exhibited a complex morphological response once a critical strain was reached 6 min after membrane stretching, demonstrating a nonmonotonic transition from creep to recovery under constant load (Figure 1D, iv). Reproducibility was validated by two independent measurements showing only statistically insignificant differences (Supplemental Figure S1A). Furthermore, the creep-recovery transition of muscle nuclei was shared by hypodermis nuclei, indicating that this nuclear property is conserved across tissues both by individual nuclei (Supplemental Figure S2) and by population averages (Figure 2A, i and ii).

Nucleus mechanics fits a tensile-compressive linear viscoelastic model

Forces propagate outside-in and inside-out between the cell nucleus and the microenvironment along cytoskeletal filaments and across the LINC complex (Buxboim *et al.*, 2010; Tajik *et al.*, 2016). Nucleoskeletal–cytoskeletal connections allow cells to regulate their contractile state, thus maintaining a linear relationship between the projected areas of the cell and the nucleus, which is an invariant property that is robust to changes in extracellular stiffness and geometry, and to myosin relaxation (Buxboim *et al.*, 2017). Cell–nucleus correlations appear to be initially satisfied also within living nematodes, showing a gradual viscoelastic increase in nucleus projected area concomitantly with the elastic stretching of the cells. However, the transition from nuclear creep to recovery was not paralleled by relaxation of the cells. Disruption of the correlation between cell and nucleus projected areas is indicative of a nucleoskeletal–cytoskeletal decoupling (NCD) as was reported recently for

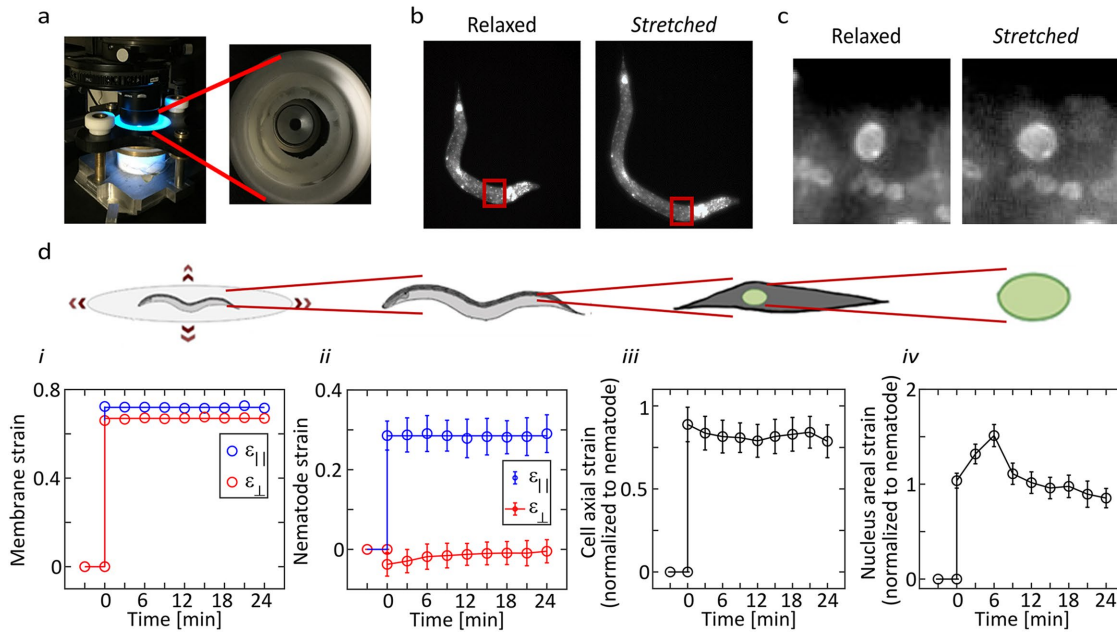


FIGURE 1: Mechanical creep test of cell nuclei within live nematodes reveals anomalous response to applied stresses. (A) Live *C. elegans* nematodes are placed between two elastic silicon membranes on a stretching apparatus mounted onto an inverted microscope. (B) Fluorescent time-lapse images of the nematodes are recorded as the membranes are being radially stretched. (C) Zoom-in images (red frames in B) of GFP-conjugated Ce-lamin nuclei show induced deformation along the primary axis of the nematode. (D) Creep test is performed by (i) maintaining a 70% radial strain of the membranes (left). Average dynamic strain profiles of the (ii) nematodes ($n = 3$), (iii) cells (estimated as the distance between proximal nuclei, $n = 7$), and (iv) nuclei ($n = 12$) are evaluated based on time-lapse imaging. Unlike nematodes and cells that exhibit a constant elastic axial deformation, nuclei respond nonmonotonically to applied stress (right).

cells in culture (Gilbert *et al.*, 2019). We thus hypothesized that creep-recovery transitions mark NCD within living nematodes as we observed in muscle and in hypodermis at comparable levels of critical nuclear strain (Figure 2A, i and ii).

To test our hypothesis that creep-recovery transition underlies NCD, we performed a creep test of the SUN-domain Unc-84-null nematodes that lack intact LINC attachments between the nucleus and the surrounding cytoskeleton (Malone *et al.*, 1999; Bone *et al.*, 2014). Strikingly, Unc84-null nuclei responded elastically to applied load, absent of nonmonotonic creep-recovery transition (Figure 2B). The absence of creep-recovery transitions only in Unc-84-null nuclei that are disconnected from their cytoskeletal surroundings strongly supports our hypothesis. While the exact mechanism and location of detachment remain unknown, we propose that NCD is a protective mechanism of living nematodes that prevents chromatin damage in nuclei under high load.

To gain insight into creep-recovery transition, we reconsidered the stresses that are applied on the nematodes during membrane stretching. Because contact is maintained during stretching between the nematodes and the top and bottom membranes, we distinguish between in-plane tensile stresses that axially pull on the nematodes and compressive forces that are vertically applied onto the nematodes as the membranes are pulled against each other (Figure 2C). Unlike compressive stresses that are applied to the nuclei independent of NCD, the transmission of tensile forces requires intact connections with the nuclear lamina (Buxboim *et al.*, 2010). We therefore formulated a linear viscoelastic model of nucleus deformation dynamics in response to tensile stresses, σ_t , and compressive stresses, σ_c (Figure 2D). The resistance to tensile stresses is modeled by a viscoelastic solid-like Kelvin-Voigt element, which is composed of a spring and dashpot connected in parallel (k_t and μ_t).

Nucleus resistance to compressive stresses is modeled using an elastic spring (k_c). Once the membranes are pulled, only k_c stretches and compressive areal strain is given by

$$\epsilon_c = -\nu \frac{\sigma_c}{k_c} \quad (1)$$

where ν is the Poisson's ratio of the nucleus that accounts for converting compressive stresses into lateral deformation (Figure 2E). Nuclear deformations due to tensile stresses, which take place only in cells with intact connections with the surrounding cytoskeleton, increase gradually due to the viscous dashpot element μ_t :

$$\epsilon_t = \frac{\sigma_t}{k_t} (1 - e^{-t/\tau}) \quad (2)$$

Here, the response time is set by the Kelvin-Voigt elements:

$$\tau = \mu_t/k_t \quad (3)$$

Because tensile and compressive strains are decoupled channels of deformation, creep strain is simply their superposition:

$$\epsilon_{\text{creep}} = \epsilon_c + \epsilon_t \quad (4)$$

Once critical strain is reached, the nucleus physically decouples from the surrounding cytoskeleton. As a result, the tensile stresses are removed, allowing viscoelastic relaxation of the Kelvin-Voigt deformations:

$$\epsilon_{\text{recov}} = \epsilon_c + \epsilon_t(t_{cr}) e^{-(t-t_{cr})/\tau} \quad (5)$$

The exact values of the applied compressive and tensile forces are unknown; however, both stresses are assumed to be proportional to the extent of whole nematode stretching. Hence, the equivalent elastic moduli were evaluated by fitting our model to the

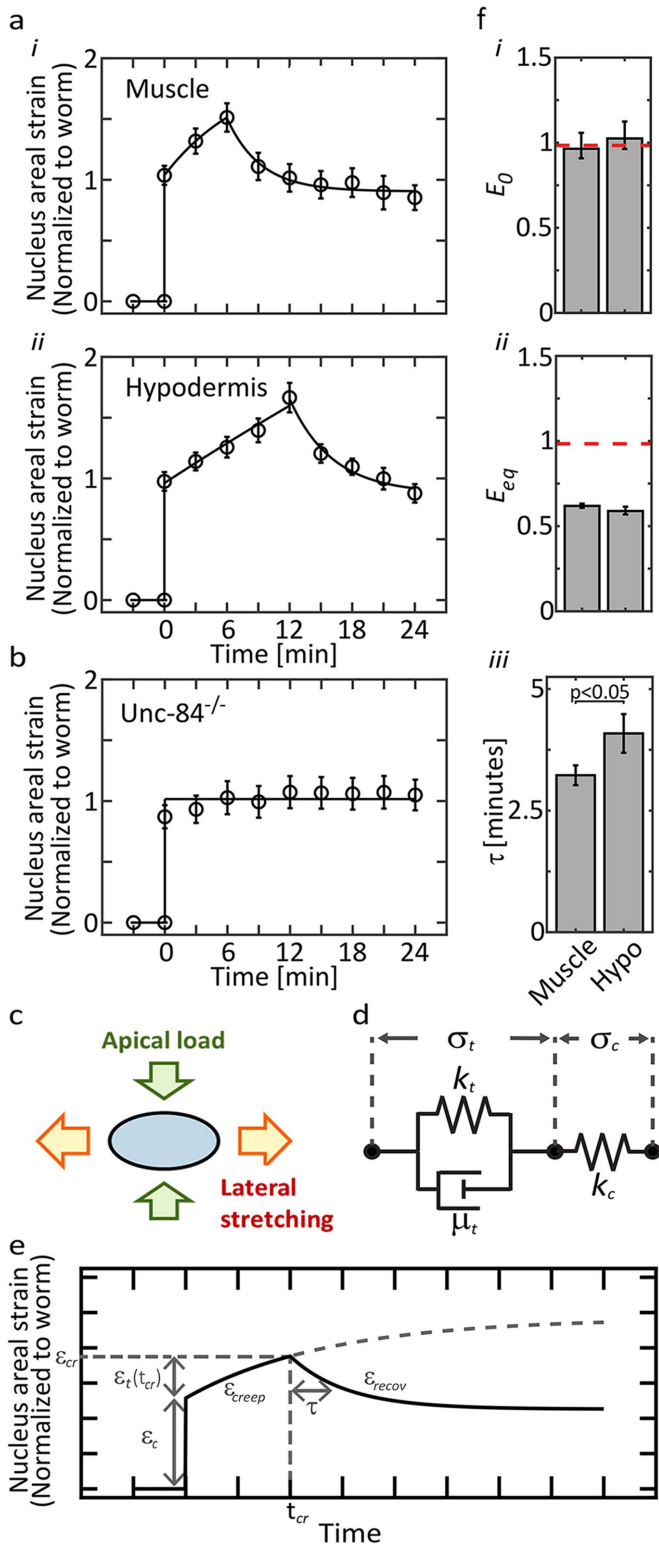


FIGURE 2: A tensile-compressive viscoelastic model of the nucleus in living nematodes. (A) Creep tests of nuclei in (i) muscle tissue (12 nuclei in two nematodes) and in (ii) hypodermis tissue (11 nuclei in two nematodes) share a nonmonotonic response to a constant load. (B) Nuclei in *Unc-84*-null nematodes (18 nuclei in four nematodes) maintain a constant deformation under a constant load. (C) Equiaxial stretching of the two membranes generates tensile stresses on the nuclei that are mediated via LINC attachments and compressive stresses that are independent of nucleoskeletal–cytoskeletal connections. (D) A minimal viscoelastic model of the nucleus

areal nuclear strain curves that we normalized by the total nematode strain in each experiment.

Our model is thus defined by fitting both creep and recovery strain regimes to evaluate the following parameters: ϵ_c , σ_t/k_t , and τ (t_{cr} is manually set). The equivalent instantaneous elastic modulus, E_0 , accounts for nucleus resistance to compressive stresses. E_0 is obtained by (Figure 2E)

$$E_0 = \epsilon_c^{-1} \quad (6)$$

Consistently, the equivalent equilibrium elastic modulus, E_{eq} , accounts for the steady-state resistance to applied stresses of the nucleus absent of NCD. E_{eq} is given by

$$E_{eq} = \left(\epsilon_c + \frac{\sigma_t}{k_t} \right)^{-1} \quad (7)$$

Finally, τ is obtained by fitting the recovery phase (Eq. 5), which consists of more data points than creep phase.

Muscle and hypodermis nuclei have similar stiffness but different viscosities

The mechanical properties of the nucleus in muscle and in hypodermis tissues were obtained by curve fitting of both creep (Eq. 4) and recovery (Eq. 5) dynamics (Figure 2A, i and ii, solid lines). R-square scoring of curve-fitting quality was 0.97 in muscle and 0.98 in hypodermis, thus supporting our nuclear model. The instantaneous elastic modulus (Eq. 6), equilibrium elastic modulus (Eq. 7), and recovery response time (Eq. 3) were then calculated for muscle and hypodermis. The equivalent elastic modulus of *Unc-84*^{-/-} nuclei was evaluated by fitting an elastic spring that accounts for compressive stresses. The instantaneous and equilibrium elastic moduli, E_0 and E_{eq} , were both equal in muscle and hypodermis nuclei (Figure 2F, i and ii). Because instantaneous deformation is determined by compressive stresses, E_0 is equal in *Unc-84* null and LINC-intact nuclei (Figure 2F, i). However, E_{eq} is lower in muscle and hypodermis nuclei because it accounts for k_0 and k_{eq} springs in series (Figure 2F, ii). Response time τ was relatively short in muscle nuclei and long in hypodermis nuclei (Figure 2F, iii). To test nucleus response under lower load, we performed a creep test of muscle nuclei within nematodes that were stretched ~15% (low load) and ~30% (high load). Nuclear strain normalized by nematode stretching, which is analogous to nuclear creep compliance, was higher under low load (Supplemental Figure S3). This suggests stress stiffening of nuclei within living nematodes, which is consistent with former measurements performed in isolated mammalian nuclei (Guilluy *et al.*, 2014) and with mechanisms that stabilize the lamina in cells in culture (Buxboim *et al.*, 2014) and strengthen the nuclear envelope (Cho *et al.*, 2019).

Lamin controls the viscoelastic properties of the nucleus

To obtain a mechanistic understanding of nucleus mechanics, we performed cytoskeletal and nucleoskeletal perturbations and studied the effect on nucleus response to applied load.

separates between tensile (σ_t) and compressive (σ_c) loads resisted by a solid-like Kelvin-Voigt module ($k_t \parallel \mu_t$) and an elastic spring (k_c), respectively. ϵ Nucleus deformation dynamics in response to applied load consists of an instantaneous elastic stretch due to compressive stresses (ϵ_c), followed by creep due to tensile stresses (ϵ_t). At critical time t_{cr} , creep strain ϵ_{creep} reaches a critical strain (ϵ_{cr}) leading to physical decoupling of the nucleus and gradual relaxation of tensile strains (ϵ_{recov}). (F) Curve-fitting evaluation of the (i) instantaneous and (ii) equilibrium elastic moduli and the (iii) viscoelastic recovery time. Red lines mark the elasticity of *Unc-84* null nuclei (k_c).

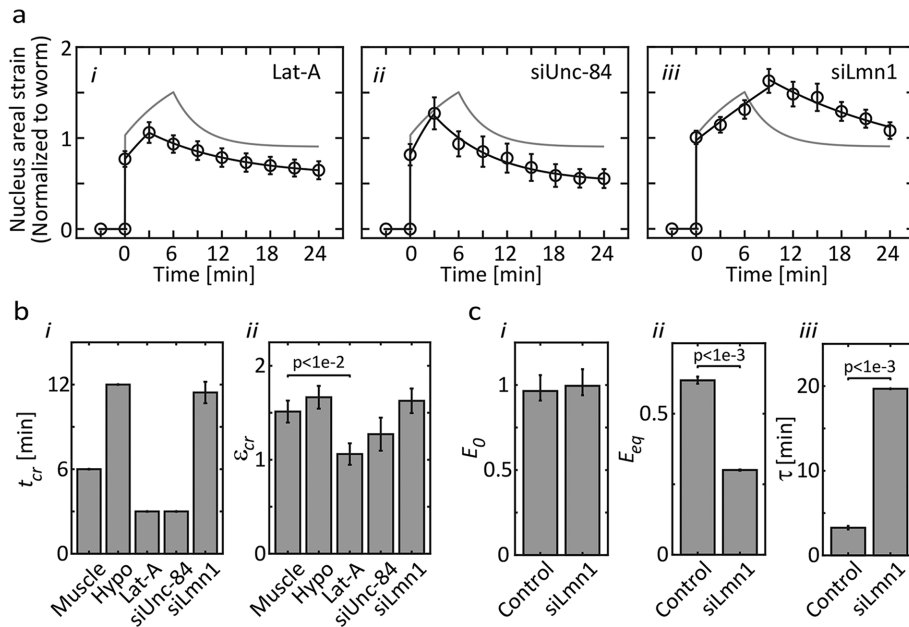


FIGURE 3: Cytoskeletal and nuclear perturbations modulate nucleus deformation dynamics in accordance with the tensile-compressive viscoelastic model. (A) Creep tests of muscle tissue nuclei in nematodes treated with (i) Lat-A (3 nematodes, 14 nuclei), (ii) siUnc-84 (3 nematodes, 14 nuclei), and (iii) siLmn-1 (4 nematodes, 16 nuclei) are fitted using the tensile-compressive model. Nontreated nucleus deformation curves are plotted in gray as reference. (B) Fitted values of (i) critical time and (ii) critical strain are shown across tissues and treatment perturbations. (C) Evaluation of the (i) instantaneous and (ii) the equilibrium elastic moduli, and (iii) viscoelastic response time. Lat-A: latrunculin-A. RNAi: RNA interference.

Filamentous actin polymerization was disrupted by treating live nematodes with latrunculin-A (Lat-A; Figure 3A, i) and decreased LINC complex attachment density by feeding the nematodes with RNA interference (RNAi) against *unc-84* (siUnc84; Figure 3A, ii). The nuclear lamina was perturbed by feeding live nematodes with RNAi against *lmn-1* (siLmn1, Figure 3A, iii). Changes to the viscoelastic properties of the nucleus were evaluated via creep test and analyzed by model fitting as described above. Compared with control nuclei (Figure 3; light gray), both actin depolymerization and partial LINC disruption led to an overall decrease in nucleus compliance (Figure 3A, i and ii). Critical strain for NCD appears to be a conserved property across tissues and invariant to nuclear perturbations. However, both cytoskeletal perturbations decreased critical time and strain compared with untreated muscle control (Figure 3B, i and ii). Relative to nonperturbed muscle nuclei, *Lmn-1* knockdown led to a shallower creep slope and a higher critical strain (Figure 3A, iii). Model fits of nucleus perturbations indicate that knockdown of *Lmn-1*, which in the nematode combines properties of both A- and B-type mammalian lamins (Liu *et al.*, 2000; Lyakhovetsky and Gruenbaum, 2014), softened the equilibrium elastic modulus twofold and prolonged response time sevenfold (Figures 3C, ii and iii). Increase in τ is consistent with a decrease in the restoring force due to softening of k_t (Figure 2F), in tune with lamin-A knockdown experiments in mammalian cells (Lammerding *et al.*, 2006) performed also by us (Wintner *et al.*, 2020).

Ageing alters long-term stiffness without significantly decreasing normalized lamin levels

C. elegans is an established model organism in the research of aging and associated laminopathic genetic disorders (Haithcock *et al.*,

2005). To study how nuclear mechanics changes with aging, we performed a creep test of L4 larvae (D0), 2-d-old (D2), and 4-d-old (D4) adult nematodes (Supplemental Figure S4A). We first compared Ce-lamin protein levels between D0, D2, and D4 nematodes via Western blotting of whole nematode lysates (Figure 4B, i). Because D0 nematodes are significantly smaller despite having an equal number of cells and nuclei as D2 and D4 nematodes (Supplemental Figure S4A), we normalized Ce-lamin intensities by (total protein)/(nematode volume). Based on three biological replicas, we excluded significant differences in Ce-lamin protein levels with aging (Supplemental Figure S4B, ii).

With aging, critical strain decreased between D0 and D2 and D4, whereas critical time was shorter in D4 nematodes, thus recapitulating the effects of cytoskeletal perturbations that we observed following actin depolymerization and LINC disruption (Figure 3B, i and ii). Both instantaneous and steady-state elastic moduli were low in young (D0) nuclei and high in aged (D2 and D4) nuclei (Figures 4A, and 3B, i and ii). Aging-associated stiffening of the nucleus was observed concomitantly with fourfold increase in the relaxation time in aged nuclei (Figure 4C, iii). Collectively, we find that ag-

ing increases the elastic resistance of nuclei under constant load and the dissipative response time required for reaching a mechanical equilibrium.

DISCUSSION

Here we present, to the best of our knowledge, the first rheology study of the cell nucleus in a live multicellular organism. Using a custom-designed worm-stretching device, we performed a creep test and identified anomalous deformation dynamics of individual nuclei. Compared with the whole nematode strain (up to 0.3), nuclei of muscle and hypodermis cells were deformed more, indicating that these are relatively soft regions within the worm. There are several examples of large deformations of cells and nuclei, including stretching of skin epidermis and dilation of smooth muscle tissue wall due to luminal filling and distension. We report on the nonmonotonic transition from creep to recovery of nuclei parallel to constant stretching of the cells that is indicative of NCD once critical strain is reached. This is experimentally supported by the elastic deformation of SUN-domain *Unc-84* knockout nuclei that lack intact LINC complex attachments. Nucleus mechanics is well modeled by a three-element linear viscoelastic material (SLS model; Guilak *et al.*, 2000) that superimposes LINC-dependent tensile stresses and LINC-independent compressive stresses. Disruption of filamentous actin polymerization and knockdown of *unc-84* do not ablate all LINC complexes but rather decrease their number. Hence, earlier NCD at lower critical strain is likely attributed to the increase in the average load per LINC attachment (Figure 3B, i and ii). The anomalous response of the nucleus to applied stresses is conserved across tissues and across conditions. LINC complex repair appears to be hindered for approximately 20 min following NCD, optionally due to retraction of the cytoskeletal filaments

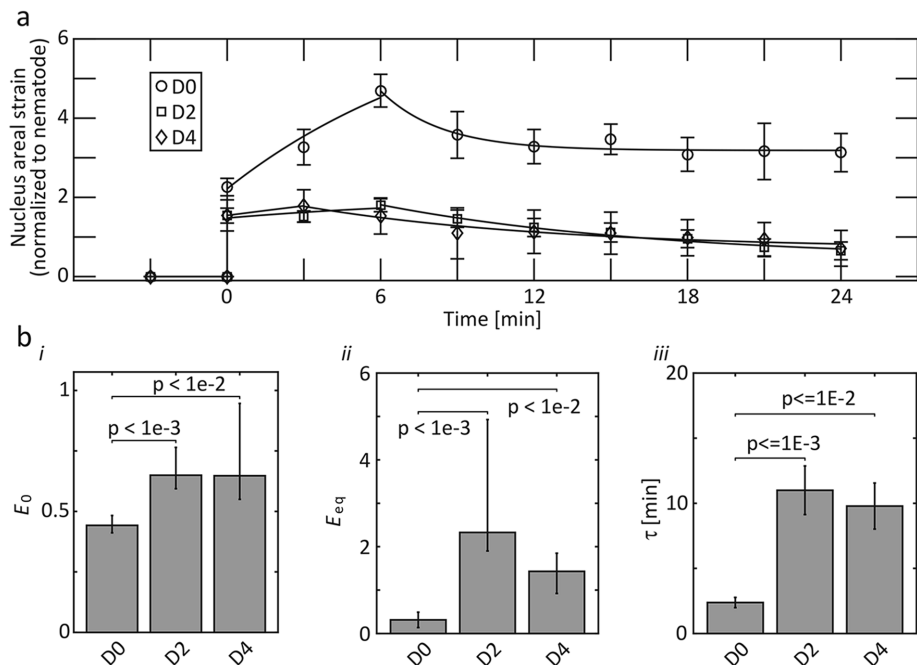


FIGURE 4: Aging alters nucleus elasticity and viscosity. (A) Nucleus strain dynamics measured on day 0 (D0: 2 nematodes, 10 nuclei), day 2 (D2: 3 nematodes, 9 nuclei), and day 4 (D4: 2 nematodes, 5 nuclei) show high compliance by nuclei of “young” compared with aged nematodes. (B) Evaluation of the (i) instantaneous and (ii) equilibrium elastic moduli, and (iii) viscoelastic response time.

away from the nucleus. Tracking LINC repair during longer time periods following NCD was impeded due to loss of nematode viability during creep test.

C. elegans nuclei exhibit aging-related modifications in nuclear morphology, which were also observed in accelerated aging disorders (Haithcock *et al.*, 2005). Here we performed a creep test of L4, and D2 and D4 adult nematodes to characterize the effects of nematode age on nucleus mechanics. We found that in aged nematodes NCD was observed earlier and at lower critical strain compared with young nematodes (Figure 4). A decrease in critical strain is consistent with nucleus stiffening and prolonged response time. Our *in vivo* measurements reproduce *in vitro* studies that report stiffening of equilibrium elasticity, which is a hallmark of the Hutchinson-Gilford progeria syndrome (HGPS) as well as normal aging in amphibian and mammalian cells (Dahl *et al.*, 2006; Verstraeten *et al.*, 2008; Kaufmann *et al.*, 2011; Apte *et al.*, 2017).

We derive a dissipative response time τ that measures the duration of viscoelastic transition toward equilibrium mechanics (Figures 2F, iii, 3C, iii, and 4D, iii). Tethering of the nucleus to the surrounding cytoskeleton was shown to slow down strain relaxation and rate of mechanical energy release owing to cytoskeletal viscosity (Wang *et al.*, 2018). The response time that we measure in live nematodes (minutes) is significantly longer than the equivalent timescales measured for isolated nuclei (<1 s; Wang *et al.*, 2018) and nuclei surrounded by cytoskeleton within intact cells (a few seconds; Swift *et al.*, 2013b; Wintner *et al.*, 2020). Rapid release of mechanical energy increases the risk of structural damage to the nucleus and the encapsulated genetic material. We find here that the actual energy release rate within a live organism is even slower than *in vitro* estimates. Hence, the physiological environment of cells and tissues provides a dissipative mechanism for protecting the nucleus and chromatin from applied forces.

METHODS

Nonaging strains and culture

We used the following *C. elegans* strains in this study: PD4810 (*lmn-1::GFP, ccls4810* [pJKL380.4 *Plmn-1::lmn-1::gfp::lmn-1* 3'UTR + pMH86 *dpy20(+)*]), YG751 (*lmn-1::GFP::unc-84* null [pJKL380.4 *Plmn-1::lmn-1::gfp::lmn-1* 3'UTR + pMH86 *dpy20(+); unc-84(e1174)*]). *C. elegans* strains were maintained and manipulated under standard conditions as previously described (Brenner, 1974). Strains were out-crossed at least three times to ensure a clean background.

Nematode culture and stretching

C. elegans strains were bleached in 0.06 M NaOH, 0.5% sodium hypochlorite solution. L1 synchronization was performed by incubating the embryos on empty nematode growth medium (NGM) plates for 18 h at 20°C. L1 nematodes were washed in M9 buffer (3 g KH_2PO_4 , 6 g Na_2HPO_4 , 5 g NaCl, 1 ml 1M MgSO_4 , H_2O to 1 l sterilize by autoclaving) and reseeded in plates containing a thin lawn of OP50/RNAi bacteria. Late L4 synchronized nematodes were collected into Eppendorf tubes and washed three times. To support adhesion, 0.2% poly-L-lysine (Sigma P2636) was added at equal volume and supplemented with 10 μl anti-fade

solution (9 parts glycerol, 1 part 10X phosphate-buffered saline, 0.1 part 20% (wt/vol) *n*-propyl gallate (Sigma P3130) in dimethyl sulfoxide). Nematodes were allowed to settle down for a few minutes.

Nematodes were transferred to the center of a 4" \times 4" square silicon sheet (cut from 12" \times 12", 0.005" NRV G/G 40D silicon membrane, SMI) in 20 separate droplets. The nematodes were then covered by a second silicone sheet and trapped air bubbles were removed. The “sandwiched” nematodes were placed on a stretching device (Zuela *et al.*, 2016) and mounted on top of an inverted microscope (Nikon Eclipse Ti-U inverted microscope, equipped with a Nikon S Plan fluor ELWS 40X/0.60 for PD4810 experiments and a Plan Apo VC 20X/0.75 for YG751 experiments). Equiaxial stretching was performed within the conjugated plane of the microscope and time-lapse recording (Andor Zyla 4.2 sCMOS camera controlled with NIS Elements 4.5.00 software) was performed both in bright field phase contrast and in fluorescence channels (Nikon Intensilight C-HGFI light source and Chroma ET-EGFP [FITC/Cy2] filter set).

Image processing, mechanical, and statistical analyses

Whole nematodes (bright field channel) and nuclei (EGFP fluorescence channel) were segmented using ImageJ. As described in the main text, projected area, contour length, and distances were calculated using ImageJ tools. Viscoelastic analyses and curve fitting were performed as described in detail in the main text using Matlab-2018a (Mathworks).

Cytoskeletal drug perturbations

Latrunculin-A (Lat-A; Sigma L5163) was freshly diluted in M9 medium at 5 mM. Five droplets (150 μl in total) were added onto the OP50 bacteria lawn of NGM plates to reach full coverage and left to dry. Synchronized L1 nematodes were placed on top of the

drug-immersed plates at 20°C for 24 h until reaching the appropriate developmental stage (late L4).

RNAi experiments

RNAi knockdown of target genes was performed via bacteria-feeding as previously described (Timmons *et al.*, 2001). *Escherichia coli* clones were obtained from the Vidal and Ahringer RNAi libraries (Kamath and Ahringer, 2003; Kim *et al.*, 2005). L4440 clone was used as an empty vector control. *lmn-1* and *unc-84* knockdown was performed using the DY3.2 and F54B11.3 vectors, respectively. Specifically, synchronization L1 nematodes were transferred to feeding plates at 20°C and experiments were performed at late L4 stage as described above.

Aging stretching experiments

Synchronized L1 PD4810 were placed on NGM plates at 20°C for 24 h, until reaching late L4 stage. Late L4 nematodes (D0) were extracted by picking for subsequent experiments. The remaining nematodes were further incubated at 20°C for an additional 12 h until reaching adult stage. Adult nematodes were transferred by picking into new NGM plates and incubated at 20°C. Two-day-old adult nematodes (D2) were extracted by picking 36 h after transfer for subsequent experiments. The remaining nematodes were transferred by picking to new NGM plates and incubated for an additional 48 h at 20°C. Four-day-old adult nematodes (D4) were then extracted by picking for subsequent experiments. Extracted nematodes were transferred into M9 droplets and placed onto an unseeded NGM plate for 10 min to remove residual OP50 bacteria. The nematodes were then transferred into a single 1 µl droplet containing 3:1 M9:anti-fade mixture and placed at the center of a 4" × 4" square silicon sheet. Nematode stretching was performed by placing a second membrane on top and mounted onto the stretching apparatus as described above. Each age group consisted of 20 nematodes.

Western blotting

To eliminate the contribution of embryonic Ce-lamin to the calibration of adult Ce-lamin levels across age groups, we used temperature-sensitive sterile CF512 nematode strain [(b26) II; fem-1(hc17) IV]. Bleached CF512 embryos were synchronized as described above. L1 nematodes were transferred to OP50 containing NGM plates and incubated at 25°C for 24 h. 150 late L4 nematodes (D0) were collected for Western blotting and the remaining nematodes were transferred to new NGM plates and incubated at 25°C (24 h) followed by 20°C (24 h). 150 2-d-old (D2) nematodes were collected for Western blotting. The remaining nematodes were transferred to new NGM plates and incubated at 20°C (48 h). 150 four-day-old (D4) nematodes were collected for Western blotting.

Western blotting was performed as previously described (Towbin *et al.*, 1979; Bank *et al.*, 2011). In short, nematode samples were washed three times in M9 buffer and immersed in 100 µl M9 buffer. Nematodes were lysed by adding a 900-µl mixture of RIPA lysis buffer (10 mM Tris-Cl, pH 8.0, 1 mM EDTA, 0.5 mM EGTA, 1% Triton X-100, 0.1% sodium deoxycholate, 0.1% SDS, 140 mM NaCl), X25 protease inhibitor (cOmplete protease inhibitor cocktail by Sigma Aldrich), and 0.1 M phenylmethylsulfonyl fluoride (PMSF; Sigma P7626) at 95:4:1 volume ratios. Nematode lysate solutions were centrifuged at 2000 rpm for 2 min. Supernatant was removed and pellet was dissolved in 200 µl RIPA-PI-PMSF lysis buffer. The samples underwent four freezing-thawing cycles in liquid nitrogen and sonication (Sonics Vibra Cell sonicator with a model CV33 microtip at 34% amplification 4 × 10 s sonication periods). Samples underwent

two freeze-thaw cycles and centrifuged at 7500 rpm for 5 min at 4°C. Supernatant was collected and transferred to a new Eppendorf tube for use.

Total protein levels were calibrated using bicinchoninic acid (BCA) assay (ThermoFisher Pierce BCA Protein Assay kit, OD measured with BioTek synergy 2 multimode multiplate reader). Samples were run on a 9% SDS polyacrylamide gel, transferred to a nitrocellulose membrane and blotted using anti-Ce-lamin antibody (Keyhole limpet hemocyanin (KLH)-conjugated C-terminal peptide of Ce-lamin; VEFSESSDPSDPADRC; serum 3932, bleed 6, dilution of 1:1000). Chemiluminescence images were acquired (Vilber Fusion FX). Ce-lamin levels were quantified by measuring total band intensities normalized to total protein levels.

ACKNOWLEDGMENTS

We thank Prof. Jan Lammerding (Cornell University) and Dr. Yonatan Tzur (Hebrew University of Jerusalem) for discussions and technical assistance. AB is greatly appreciative of the support from the Israel Science Foundation (Grant Number 1246/14), the European Research Council (ERC-StG 678977), the United States – Israel bi-national science foundation (BSF StG 2017357) and the Niedersächsisches Vorab (Grant No. ZN 3183).

REFERENCES

- Apte K, Stick R, Radmacher M (2017). Mechanics in human fibroblasts and progeria: lamin A mutation E145K results in stiffening of nuclei. *J Mol Recognit* 30, e2580.
- Athirasala A, Hirsch N, Buxboim A (2017). Nuclear mechanotransduction: sensing the force from within. *Curr Opin Cell Biol* 46, 119–127.
- Bank EM, Ben-Harush K, Wiesel-Motiuk N, Barkan R, Feinstein N, Lotan O, Medalia O, Gruenbaum Y (2011). A laminopathic mutation disrupting lamin filament assembly causes disease-like phenotypes in *Caenorhabditis elegans*. *Mol Biol Cell* 22, 2716–2728.
- Bone CR, Tapley EC, Gorjanacz M, Starr DA (2014). The *Caenorhabditis elegans* SUN protein UNC-84 interacts with lamin to transfer forces from the cytoplasm to the nucleoskeleton during nuclear migration. *Mol Biol Cell* 25, 2853–2865.
- Brenner S (1974). The genetics of *Caenorhabditiselegans*. *Genetics* 77, 71–94.
- Buxboim A, Irianto J, Swift J, Athirasala A, Shin JW, Rehfeldt F, Discher DE (2017). Coordinated increase of nuclear tension and lamin-A with matrix stiffness outcompetes lamin-B receptor that favors soft tissue phenotypes. *Mol Biol Cell* 28, 3333–3348.
- Buxboim A, Ivanovska IL, Discher DE (2010). Matrix elasticity, cytoskeletal forces and physics of the nucleus: how deeply do cells ‘feel’ outside and in? *J Cell Sci* 123, 297–308.
- Buxboim A, Swift J, Irianto J, Spinler KR, Dingal PC, Athirasala A, Kao YR, Cho S, Harada T, Shin JW, Discher DE (2014). Matrix elasticity regulates lamin-A,C phosphorylation and turnover with feedback to actomyosin. *Curr Biol* 24, 1909–1917.
- Cho S, Vashisth M, Abbas A, Majkut S, Vogel K, Xia Y, Ivanovska IL, Irianto J, Tewari M, Zhu K, *et al.* (2019). Mechanosensing by the lamina protects against nuclear rupture, DNA damage, and cell-cycle arrest. *Dev Cell* 49, 920–935.e925.
- Dahl KN, Engler AJ, Pajerowski JD, Discher DE (2005). Power-law rheology of isolated nuclei with deformation mapping of nuclear substructures. *Biophys J* 89, 2855–2864.
- Dahl KN, Scaffidi P, Islam MF, Yodh AG, Wilson KL, Misteli T (2006). Distinct structural and mechanical properties of the nuclear lamina in Hutchinson-Gilford progeria syndrome. *Proc Natl Acad Sci USA* 103, 10271–10276.
- Denais CM, Gilbert RM, Isermann P, McGregor AL, te Lindert M, Weigel B, Davidson PM, Friedl P, Wolf K, Lammerding J (2016). Nuclear envelope rupture and repair during cancer cell migration. *Science* 352, 353–358.
- Furusawa T, Rochman M, Taher L, Dimitriadis EK, Nagashima K, Anderson S, Bustin M (2015). Chromatin decompaction by the nucleosomal binding protein HMGN5 impairs nuclear sturdiness. *Nat Commun* 6, 6138.
- Gettner SN, Kenyon C, Reichardt LF (1995). Characterization of beta pat-3 heterodimers, a family of essential integrin receptors in *C. elegans*. *J Cell Biol* 129, 1127–1141.

- Gilbert HTJ, Mallikarjun V, Dobre O, Jackson MR, Pedley R, Gilmore AP, Richardson SM, Swift J (2019). Nuclear decoupling is part of a rapid protein-level cellular response to high-intensity mechanical loading. *Nat Commun* 10, 4149.
- Gonzalez-Bermudez B, Guinea GV, Plaza GR (2019). Advances in micropipette aspiration: applications in cell biomechanics, models, and extended studies. *Biophys J* 116, 587–594.
- Guilak F, Tedrow JR, Burgkart R (2000). Viscoelastic properties of the cell nucleus. *Biochem Biophys Res Commun* 269, 781–786.
- Guilluy C, Osborne LD, Van Landeghem L, Sharek L, Superfine R, Garcia-Mata R, Burrigke K (2014). Isolated nuclei adapt to force and reveal a mechanotransduction pathway in the nucleus. *Nat Cell Biol* 16, 376–381.
- Haithcock E, Dayani Y, Neufeld E, Zahand AJ, Feinstein N, Mattout A, Gruenbaum Y, Liu J (2005). Age-related changes of nuclear architecture in *Caenorhabditis elegans*. *Proc Natl Acad Sci USA* 102, 16690–16695.
- Heo SJ, Driscoll TP, Thorpe SD, Nerurkar NL, Baker BM, Yang MT, Chen CS, Lee DA, Mauck RL (2016). Differentiation alters stem cell nuclear architecture, mechanics, and mechano-sensitivity. *Elife* 5, e18207.
- Hochmuth RM (2000). Micropipette aspiration of living cells. *J Biomech* 33, 15–22.
- Irianto J, Xia Y, Pfeifer CR, Athirasala A, Ji J, Alvey C, Tewari M, Bennett RR, Harding SM, Liu AJ, et al. (2017). DNA damage follows repair factor depletion and portends genome variation in cancer cells after pore migration. *Curr Biol* 27, 210–223.
- Kamath RS, Ahringer J (2003). Genome-wide RNAi screening in *Caenorhabditis elegans*. *Methods* 30, 313–321.
- Kaufmann A, Heinemann F, Radmacher M, Stick R (2011). Amphibian oocyte nuclei expressing lamin A with the progeria mutation E145K exhibit an increased elastic modulus. *Nucleus* 2, 310–319.
- Kim JK, Gabel HW, Kamath RS, Tewari M, Pasquinelli A, Rual JF, Kennedy S, Dybbs M, Bertin N, Kaplan JM, et al. (2005). Functional genomic analysis of RNA interference in *C. elegans*. *Science* 308, 1164–1167.
- Krause M, Te Riet J, Wolf K (2013). Probing the compressibility of tumor cell nuclei by combined atomic force-confocal microscopy. *Phys Biol* 10, 065002.
- Lammerding J, Fong LG, Ji JY, Reue K, Stewart CL, Young SG, Lee RT (2006). Lamins A and C but not lamin B1 regulate nuclear mechanics. *J Biol Chem* 281, 25768–25780.
- Lammerding J, Lee RT (2009). Mechanical properties of interphase nuclei probed by cellular strain application. *Methods Mol Biol* 464, 13–26.
- Lherbette M, Dos Santos A, Hari-Gupta Y, Fili N, Toseland CP, Schaap IAT (2017). Atomic force microscopy micro-rheology reveals large structural inhomogeneities in single cell-nuclei. *Sci Rep* 7, 8116.
- Liu J, Rolef Ben-Shahar T, Riemer D, Treinin M, Spann P, Weber K, Fire A, Gruenbaum Y (2000). Essential roles for *Caenorhabditis elegans* lamin gene in nuclear organization, cell cycle progression, and spatial organization of nuclear pore complexes. *Mol Biol Cell* 11, 3937–3947.
- Lyakhovetsky R, Gruenbaum Y (2014). Studying lamins in invertebrate models. *Adv Exp Med Biol* 773, 245–262.
- Malone CJ, Fixsen WD, Horvitz HR, Han M (1999). UNC-84 localizes to the nuclear envelope and is required for nuclear migration and anchoring during *C. elegans* development. *Development* 126, 3171–3181.
- Pajeroski JD, Dahl KN, Zhong FL, Sammak PJ, Discher DE (2007). Physical plasticity of the nucleus in stem cell differentiation. *Proc Natl Acad Sci USA* 104, 15619–15624.
- Raab M, Gentili M, de Belly H, Thiam HR, Vargas P, Jimenez AJ, Lautenschlaeger F, Voituriez R, Lennon-Dumenil AM, Manel N, Piel M (2016). ESCRT III repairs nuclear envelope ruptures during cell migration to limit DNA damage and cell death. *Science* 352, 359–362.
- Rowat AC, Foster LJ, Nielsen MM, Weiss M, Ipsen JH (2005). Characterization of the elastic properties of the nuclear envelope. *J R Soc Interface* 2, 63–69.
- Shimamoto Y, Tamura S, Masumoto H, Maeshima K (2017). Nucleosome-nucleosome interactions via histone tails and linker DNA regulate nuclear rigidity. *Mol Biol Cell* 28, 1580–1589.
- Stephens AD, Banigan EJ, Adam SA, Goldman RD, Marko JF (2017). Chromatin and lamin A determine two different mechanical response regimes of the cell nucleus. *Mol Biol Cell* 28, 1984–1996.
- Stephens AD, Banigan EJ, Marko JF (2018). Separate roles for chromatin and lamins in nuclear mechanics. *Nucleus* 9, 119–124.
- Swift J, Harada T, Buxboim A, Shin JW, Tang HY, Speicher DW, Discher DE (2013a). Label-free mass spectrometry exploits dozens of detected peptides to quantify lamins in wildtype and knockdown cells. *Nucleus* 4, 450–459.
- Swift J, Ivanovska IL, Buxboim A, Harada T, Dingal PC, Pinter J, Pajeroski JD, Spinler KR, Shin JW, Tewari M, et al. (2013b). Nuclear lamin-A scales with tissue stiffness and enhances matrix-directed differentiation. *Science* 341, 1240104.
- Tajik A, Zhang Y, Wei F, Sun J, Jia Q, Zhou W, Singh R, Khanna N, Belmont AS, Wang N (2016). Transcription upregulation via force-induced direct stretching of chromatin. *Nat Mater* 15, 1287–1296.
- Timmons L, Court DL, Fire A (2001). Ingestion of bacterially expressed dsRNAs can produce specific and potent genetic interference in *Caenorhabditis elegans*. *Gene* 263, 103–112.
- Towbin H, Staehelin T, Gordon J (1979). Electrophoretic transfer of proteins from polyacrylamide gels to nitrocellulose sheets: procedure and some applications. *Proc Natl Acad Sci USA* 76, 4350–4354.
- Verstraeten VL, Ji JY, Cummings KS, Lee RT, Lammerding J (2008). Increased mechanosensitivity and nuclear stiffness in Hutchinson-Gilford progeria cells: effects of farnesyltransferase inhibitors. *Aging Cell* 7, 383–393.
- Wang X, Liu H, Zhu M, Cao C, Xu Z, Tsatskis Y, Lau K, Kuok C, Filleter T, McNeill H, et al. (2018). Mechanical stability of the cell nucleus—roles played by the cytoskeleton in nuclear deformation and strain recovery. *J Cell Sci* 131.
- Wintner O, Hirsch-Attas N, Schlossberg M, Brofman F, Friedman R, Kupervaser M, Kitsberg D, Buxboim A (2020). A unified linear viscoelastic model of the cell nucleus defines the mechanical contributions of lamins and chromatin. *Adv Sci (Weinh)* 7, 1901222.
- Zuela N, Zwerger M, Levin T, Medalia O, Gruenbaum Y (2016). Impaired mechanical response of an EDMD mutation leads to motility phenotypes that are repaired by loss of prenylation. *J Cell Sci* 129, 1781–1791.